Two center shell model with Woods-Saxon potentials: adiabatic and diabatic states in fusion

A. Diaz-Torres [a,b] and W. Scheid [b]

[a]*Institut für Theoretische Physik der Johann Wolfgang Goethe–Universität Frankfurt, Max von Laue Str. 1, D–60438 Frankfurt am Main, Germany*

[b]*Institut für Theoretische Physik der Justus–Liebig–Universität Giessen, Heinrich–Buff–Ring 16, D–35392 Giessen, Germany*

Abstract

A realistic two-center shell model for fusion is proposed, which is based on two spherical Woods-Saxon potentials and the potential separable expansion method. This model describes the single-particle motion in a fusing system. A technique for calculating stationary diabatic states is suggested which makes use of the formal definition of those states, i.e., they minimize the radial nonadiabatic coupling between the adiabatic states. As an example the system $^{16}O + {}^{40}Ca \rightarrow {}^{56}Ni$ is discussed.

Key words: Two-center shell model, Woods-Saxon potential, potential separable expansion method, adiabatic and diabatic single-particle states, fusion
PACS: 21.60.Cs, 21.10.Pc, 24.10.Cn, 25.70.Jj

1 Introduction

The two-center shell model (TCSM) is a basic microscopic model to describe the single-particle (sp) motion during a heavy ion collision near the Coulomb barrier. The sp energies and wave functions are obtained solving the Schrödinger equation with a phenomenological two-center mean field potential. This approach was first introduced by the Frankfurt school [1,2] and most of its applications so far in fission and fusion have been based on a double oscillator potential [3]. Improved versions of TCSM based on oscillator potentials have been developed for dealing with very asymmetric fission [4] and with

asymmetric fragmentations involving deformed fragments [5]. The two-center problem for realistic finite depth potentials has been solved with the wave function expansion method (usual diagonalization procedure) in Refs. [6,7]. The authors of Ref. [6] made use of two spherical Woods-Saxon potentials for describing the polarization of sp states in peripheral transfer reactions like ^{40}Ca + ^{16}O and ^{208}Pb + ^{12}C, while in Ref. [7] two deformed Gaussian potentials were applied for the fusion of a deformed and arbitrarily orientated ^{13}C projectile on the ^{16}O target.

In the present work the two-center problem is solved using two Woods-Saxon (WS) potentials and the potential separable expansion (PSE) method proposed by Revai [8,9,10,11]. In contrast to Refs.[10,11], where the PSE technique was employed within the two-center framework to describe the sp motion in peripheral collisions (the WS potential parameters were kept fixed) like ^{16}O + ^{16}O, ^{17}O + ^{13}C and ^{17}O + ^{16}O, we now extend the potential ansatz for large overlap between the nuclei by conserving the volume of the system during the amalgamation process. For the sake of simplicity, we will use two spherical WS potentials, whose parameters in a realistic calculation have to be adjusted so as to fit the experimental sp spectra around the Fermi level for the separated nuclei and for the spherical compound nucleus. For intermediate internuclear distances these parameters can be interpolated as we will discuss below. The present TCSM has the following advantages compared to the traditional one based on two oscillator potentials [2]: (i) very asymmetric reactions can be described as those used to form superheavy elements (e.g., ^{40}Ca + ^{208}Pb) without assumptions regarding the shape of the potential barrier between the fragments, (ii) the relative level positions in the colliding nuclei are correct, (iii) the two-center potential barrier between the nuclei is realistic, (iv) the Coulomb interaction for protons can be explicitly included, (v) the sp wave functions have a correct asymptotic behaviour [10], and (vi) the continuum states like Gamow resonances can be included [11] which is relevant in reactions involving drip-line nuclei. It is worth mentioning that the PSE method has also been used in conjunction with both the one-center problem [12,13] and the two-center problem [14] for nuclear structure studies.

In sect. 2, the PSE method to solve the adiabatic two-center problem is briefly presented along with the method to ensure the volume conservation of the fusing system. The adiabatic or Born-Oppenheimer approximation is based on the idea that the relative motion of the nuclei is much slower than the sp motion, so at each fixed internuclear distance the molecular sp wave functions diagonalize the two-center sp hamiltonian. These states are called *adiabatic* sp states and the nucleons occupy the lowest sp energy levels in the two-center potential. The coupling between the adiabatic sp states, called *nonadiabatic coupling*, is induced by the kinetic energy operator related to the relative motion of the nuclei. When the adiabatic sp states are well separated, this coupling may be negligible and the adiabatic approximation is adequate. Whenever the energy

2

separation between two adiabatic sp states becomes small or vanishes, the coupling may be large and the adiabatic approximation breaks down. In this case, the sp state is a linear combination of adiabatic states. In such a situation a useful approach, called stationary diabatic approximation, achieves the separation between the sp motion and the relative motion of the nuclei. The stationary *diabatic* sp states minimize the *radial* nonadiabatic coupling [15]. In the last part of sect. 2, we describe a technique to calculate the stationary diabatic sp states following this formal definition. The convenience of the diabatic sp states in the entrance phase of heavy ion collisions around the Coulomb barrier was discussed by Cassing and Nörenberg in Ref. [16]. In contrast to the adiabatic sp motion, nucleons with a diabatic motion do not always occupy the lowest energy levels, but remain in their diabatic levels during a collective motion of the system. The use of the diabatic states accounts for the main part of the coherent coupling between collective and intrinsic degrees of freedom. Very recently in Ref. [17] these states were applied for the modelling of the compound nucleus formation in the fusion of heavy nuclei. In sect. 3 numerical results for $^{16}\text{O} + {}^{40}\text{Ca} \rightarrow {}^{56}\text{Ni}$ are discussed, while conclusions are drawn in sect. 4.

2 The TCSM

We will follow the method proposed by Gareev et al. in Ref. [10] and also used by Milek and Reif in Ref. [11], which is based on the *expansion of potentials* in terms of, e.g., harmonic oscillator functions (PSE method), i.e, $V \approx \sum_{ij}^{N} |i> V_{ij} <j| \equiv V_{sep}$. The accuracy of the results obtained depends only on the accuracy of the expansion of the WS potentials. The Schrödinger equation with approximate potentials V_{sep} is solved exactly.

The finite depth nuclear potential belongig to each fragment ($s = 1, 2$) is chosen to be the following spherical WS with a spin-orbit term

$$V_s(r) = -V_{0s}f^s(r) + \frac{1}{2}\lambda_s(\frac{\hbar}{m_0 c})^2 V_{0s}\frac{1}{r}\frac{df^s_{so}}{dr}(\mathbf{l}\cdot\mathbf{s}), \tag{1}$$

where $\hbar/m_0 c = 0.21$ fm, f and f_{so} are the same function, but with different parameters, i.e., $f^s_{(so)}(r) = \{1 + \exp[(r - R^s_{0(so)})/a^s_{0(so)}]\}^{-1}$. For protons, the Coulomb potential V^s_{Coul} is taken to be that of a uniformly charged sphere with charge $Z_s e$ (Z_s being the total charge of each fragment) and the radius R^s_c, which is added to expression (1). The potentials (1) are placed at the position $\mathbf{R_s}$ in the center of mass system and thus the two-center potential reads as

$$V = e^{-i\mathbf{R}_1\hat{k}}\, V_1\, e^{i\mathbf{R}_1\hat{k}} + e^{-i\mathbf{R}_2\hat{k}}\, V_2\, e^{i\mathbf{R}_2\hat{k}}, \tag{2}$$

3

where $\hat{k} = \hbar^{-1}\hat{p}$ is the sp wave-number operator. Each potential (1) is then represented approximately (V_{sep}^s) within a truncated sp harmonic oscillator basis, $\{|\nu>, \nu = 1, \ldots N\}$, with the spin-angular part coupled to the total angular momentum j with projection m, e.g., in the momentum representation

$$|\nu> = |nljm> = g_{nl}(k) \cdot [i^{-l} Y_l(\hat{\mathbf{k}}) \otimes \chi_{\frac{1}{2}}(s)]_m^j. \tag{3}$$

The harmonic oscillator basis has the advantage that all matrix elements needed can be calculated analytically (e.g., see Appendix A in Ref. [11]) and this basis adopts essentially the same mathematical form in momentum and coordinate representations. In the coordinate representation (spherical coordinates), the radial part of the harmonic oscillator wave function can be written as $< r|nl> = h_{osc}^{-3/2}\phi_{nl}(x)$, where h_{osc} is the oscillator length and the adimensional $x = h_{osc}^{-1} r$. In the momentum representation, $< k|nl> \equiv g_{nl}(k) = (-1)^n i^l h_{osc}^{3/2} \phi_{nl}(\xi)$ being the adimensional $\xi = h_{osc} k$. The phase factor i^{-l} in the definition of the basis set (3) removes the imaginarity of $g_{nl}(k)$. The function ϕ_{nl} is the reduced oscillator function, i.e.,

$$\phi_{nl}(\xi) = \sqrt{\frac{2n!}{\Gamma(n+l+1/2)}} \cdot \xi^l \cdot e^{-\xi^2/2} \cdot L_n^{l+1/2}(\xi^2), \tag{4}$$

where $L_n^{l+1/2}(\xi^2)$ is a Laguerre polynomial. According to Ref. [19], the oscillator lenght h_{osc}^s associated with each basis set can be calculated with the expression $h_{osc}^s = 0.84 \cdot R_0^s \cdot A_s^{-1/6}$, being A_s the mass number of each fragment.

Volume conservation. To describe the amalgamation process of the two nuclei, the potential parameters have to be interpolated between their values for the separated nuclei and the spherical compound nucleus. The parameters can be correlated by assuming the condition that the volume enclosed by certain equipotential surface V_0 of the two-center potential V is conserved for all values of R, i.e.,

$$\int dv \, \Theta(V_0 - V) = v_0, \tag{5}$$

where Θ is the Heaviside step function, V_0 the fixed equipotential surface corresponding to the Fermi level of the fused system, and v_0 the volume enclosed by the equipotential surface V_0. As the two-center potential V in (5), we use $\widetilde{V_1} + \widetilde{V_2}$ where $\widetilde{V_s}$ refers to the first term of (1), i.e., the spin-orbit part is neglected. For the sake of simplicity, we will assume that the nuclear shape is the same for neutrons and protons.

The parameters $\mathcal{P} = \{V_{0s}, R_{0(so)}^s, a_{0(so)}^s, \lambda_s, R_c^s, Z_s\}$ are interpolated by means

of the unknown function $y(R)$ [7]

$$\mathcal{P}(R) = \mathcal{P}(R = 0) \left[1 - y(R)\right] + \mathcal{P}(R \to \infty) \, y(R), \tag{6}$$

where $y(R)$ satisfies the boundary conditions $y(R = 0) = 0$ and $y(R \to \infty) = 1$. The function $y(R) \in [0, 1]$ is numerically calculated by inserting (6) into (5) and requiring the conservation of the volume. The parameters $\mathcal{P}(R \to \infty)$ are unambiguously found fitting the experimental sp spectra around the Fermi level for the separated nuclei, but this is not the case for the individual fragment potentials at $R = 0$ where only the sp spectra of the compound system are known. At $R = 0$ we adopt that $R_{0(so)}^s, a_{0(so)}^s, \lambda_s$ and R_c^s are the same as those for the compound nucleus, but $V_{01} + V_{02} = V_0^{CN}$ and $Z_1 + Z_2 = Z_{CN}$. A new parameter $\alpha = V_{01}/V_0^{CN} = Z_1/Z_{CN}$ is introduced and it determines the values of V_{0s} and Z_s at $R = 0$. This $\alpha \in (0, 1)$ parameter is chosen in such a way that the splitting of the sp levels for small R is similar to that in the Nilsson model.

Adiabatic states. In the present method the two-center problem is solved in the momentum representation. The approximate potential V_{sep}^s reads as

$$V_{sep}^s = \sum_{\nu,\mu=1}^{N} |s\nu > V_{\nu\mu}^s < s\mu|, \tag{7}$$

where $\nu, \mu = \{nljm\}$. The number N of basis states included in the expansion (7) is defined by l_{max} (number of partial waves in which the potential acts) and n_{max} (the number of separable terms in each partial wave). The values of l_{max} and n_{max} are determined by the convergence of the sp energies which is accelerated using the technique of the Lanczos σ-factors [18]. For bound states the formal solution of the Schrödinger equation is as follows

$$|\varphi> = G_0(E)V|\varphi>, \quad G_0(E) = (E - \frac{\hbar^2 \hat{k}^2}{2m_0})^{-1}, \tag{8}$$

where G_0 is the Green operator for the free sp motion. Inserting (2) and (7) into (8), the expression (8) reads as

$$|\varphi> = G_0(E) \sum_{\nu,\mu=1}^{N} \sum_{s=1}^{2} V_{\nu\mu}^s \, A_{s\mu} \, e^{-i\mathbf{R}_s \hat{k}} \, |s\nu>, \tag{9}$$

where

$$A_{s\mu} = < s\mu|e^{i\mathbf{R}_s \hat{k}}|\varphi> . \tag{10}$$

The coefficients $A_{s\mu}$ are the amplitude of the molecular sp wave function $|\varphi>$ with respect to the moving basis states located at $\mathbf{R}_s$. Multiplying (9) from the left by $<s\mu|e^{i\mathbf{R}_s\hat{k}}$ and with (10), the following set of linear algebraic equations for the coefficients $A_{s\mu}$ is obtained:

$$\sum_{\mu'=1}^{N}\sum_{s'=1}^{2}[\delta_{ss'}\delta_{\mu\mu'} - \sum_{\nu=1}^{N} <s\mu|G_0(E)e^{i(\mathbf{R}_s-\mathbf{R}_{s'})\hat{k}}|s'\nu> \ V_{\nu\mu'}^{s'}] \ A_{s'\mu'} \ = 0. \ (11)$$

The solvability condition of the system (11) is that its determinant vanishes. This determines the energy eigenvalues E which appear as a parameter in the matrix elements containing G_0. With the eigenvalues E, the eigenvectors $|\varphi>$ are obtained solving the system (11) for the coefficients $A_{s\mu}$ and requiring the normalization of the state vectors $|\varphi>$. These states are the adiabatic sp states.

The quantum numbers denoting the molecular sp states arise from the symmetry properties of the two-center problem. Since the potential (2) is invariant around the axis connecting the centers of both potentials $(\mathbf{R} = \mathbf{R}_1 - \mathbf{R}_2)$, the projection of the total angular momentum j along this axis denoted by Ω is conserved. This axis is chosen as the quantization axis and the sp levels are labelled by Ω and an additional index $indx$ that distinguishes different states with the same Ω. The index $indx$ could refer either to the asymptotically good quantum numbers $(\tilde{n}lj)$ of the state to which the level goes for large R or just to an index $\tilde{n}$ counting the levels. In the intrinsic (or rotating) molecular reference frame $(\mathbf{R}_1 = \mathbf{R}$ and $\mathbf{R}_2 = 0)$ the matrix elements containing G_0 are as follows $(\hat{j} = (2j+1)^{1/2})$

$$s = s': \quad <nlj\Omega|G_0(E)|n'l'j'\Omega'> = \delta_{ll'}\delta_{jj'}\delta_{\Omega\Omega'} \ <nl|G_0(E)|n'l'>, \quad (12)$$

$s \neq s'$:

$$<nlj\Omega|G_0(E)e^{i\mathbf{R}_{ss'}\hat{k}}|n'l'j'\Omega'> = \delta_{\Omega\Omega'}(-1)^{\Omega+\frac{1}{2}} \cdot \sum_L i^{L+l-l'}$$

$$Q_{ss'} \ \hat{l}\hat{j}\hat{l}'\hat{j}' \ (l0l'0|L0)(j\Omega j'-\Omega|L0) \begin{Bmatrix} L & l' & l \\ \frac{1}{2} & j & j' \end{Bmatrix}$$

$$<nl|G_0(E) \ j_L(kR)|n'l'>, \quad (13)$$

where

$$Q_{ss'} = \begin{cases} 1, & ss' = 12 \\ (-1)^L, & ss' = 21 \end{cases}, \quad (14)$$

$$< nl|G_0(E)|n'l' >= -\frac{2m_0}{\hbar^2} \int\limits_0^\infty \frac{g_{nl}^*(k)g_{n'l'}(k)}{k^2 + \gamma^2}\ k^2 dk, \quad \gamma^2 = -\frac{2m_0E}{\hbar^2}, \quad (15)$$

$$< nl|G_0(E)\ j_L(kR)|n'l' >= -\frac{2m_0}{\hbar^2} \int\limits_0^\infty \frac{g_{nl}^*(k)g_{n'l'}(k)j_L(kR)}{k^2 + \gamma^2}\ k^2 dk. \quad (16)$$

In (16) j_L refers to the spherical Bessel function. The matrix elements (13) are obtained using (i) the expansion of $e^{i\mathbf{R}_{ss'}\mathbf{k}}$ in terms of the spherical functions

$$e^{i\mathbf{R}_{ss'}\mathbf{k}} = 4\pi \sum_{L=0}^\infty \sum_{M=-L}^L i^L j_L(kR_{ss'})Y_{LM}^*(\hat{\mathbf{R}}_{ss'})Y_{LM}(\hat{\mathbf{k}}), \quad (17)$$

and (ii) general properties of the angular momentum algebra [20].

The sp states $|indx\ \Omega >$ calculated with (11)-(16) refer to adiabatic molecular sp states in the intrinsic (or rotating) reference frame, where the amplitude of the molecular wave functions solving (11) are denoted by $B_{s\beta\Omega}$ with $\beta = \{nlj\}$. Please note that these amplitudes depend only on the relative distance R. They are independent of the orientation angles $\hat{R}$ of the molecular axis, since these are no longer contained in the matrix elements (12)-(16). The rotation of the molecular axis with respect to a space-fixed axis is then included in (9) by means of the Wigner $D_{m\Omega}^j(\hat{R})$ rotation matrices, so the $|indx\ \Omega >$ adiabatic molecular sp states in the laboratory reference frame read as follows

$$|indx\ \Omega >= G_0(E_{indx,\Omega}) \sum_{\beta m, \beta'} \sum_{s=1}^2 V_{\beta m\beta'\Omega}^s\ B_{s\beta'\Omega}\ D_{m\Omega}^j(\hat{R})\ e^{-i\mathbf{R}_s\hat{k}}\ |s\beta m >.$$
$$(18)$$

Stationary diabatic states. A natural way of introducing the stationary diabatic sp states is to impose the condition that the radial coupling operator $(-i\hbar\partial/\partial R + \mathcal{A})$ be zero or negligibly small in these states [15], where $\mathcal{A}$ identifies and cancels that spurious portion of the coupling induced by $-i\hbar\partial/\partial R$ that represents merely the translation of basis functions along with moving nuclei. Fortunately only inspection is needed to remove from the $-i\hbar\partial/\partial R$ matrix *that part which corresponds simply to displacement*, as we will show next. Then what remains after such background correction is the actual nonadiabatic coupling which vanishes for large internuclear distances. The diabatic representation is obtained by diagonalization of this coupling in a truncated set of the adiabatic sp states (18) with the same quantum number Ω, i.e., $< indx\ \Omega|(-i\hbar\partial/\partial R + \mathcal{A})|indx'\ \Omega >$. Only couplings between neighbouring levels ($indx' = indx \pm 1$) are included. In defining the matrix of the radial

nonadiabatic couplings that is diagonalized, we neglect the couplings whose strength is smaller than a threshold value γ_{thr}. The value of γ_{thr} used in the calculations should lead to the isolation of the strongest radial nonadiabatic couplings. Strong radial nonadiabatic couplings are expected to occur at the avoided crossing of the adiabatic molecular sp levels.

The adiabatic molecular sp states (18) can be re-written as

$$|indx \ \Omega>= G_0(E_{indx,\Omega})\{\sum_{\nu=1}^{N_1} C_{1\nu}^{\Omega} e^{-i\mathbf{R}\hat{k}} \ |1\nu> + \sum_{\nu=1}^{N_2} C_{2\nu}^{\Omega}|2\nu>\}, \tag{19}$$

where the coefficients $C_{s\nu}^{\Omega} = \sum_{\beta'} V_{\nu\beta'\Omega}^s B_{s\beta'\Omega}$. Here, we identify $\nu = \{\beta m\}$ and the Wigner rotation matrices are now included in the basis $|s\nu>$. The radial derivative $\partial/\partial R$ of (19) is as follows

$$\frac{\partial}{\partial R}|indx \ \Omega>= \frac{\partial G_0(E_{indx,\Omega})}{\partial R}\{\sum_{\nu=1}^{N_1} C_{1\nu}^{\Omega} e^{-i\mathbf{R}\hat{k}} \ |1\nu> + \sum_{\nu=1}^{N_2} C_{2\nu}^{\Omega}|2\nu>\}$$
$$+ G_0(E_{indx,\Omega})\{\sum_{\nu=1}^{N_1} \frac{\partial C_{1\nu}^{\Omega}}{\partial R} e^{-i\mathbf{R}\hat{k}} \ |1\nu> + \sum_{\nu=1}^{N_2} \frac{\partial C_{2\nu}^{\Omega}}{\partial R} \ |2\nu>\}$$
$$+ G_0(E_{indx,\Omega})\sum_{\nu=1}^{N_1} C_{1\nu}^{\Omega} \frac{\partial e^{-i\mathbf{R}\hat{k}}}{\partial R} \ |1\nu> . \tag{20}$$

The last term of (20) is responsible for the unphysical effect (i.e. non vanishing asymptotic couplings owing to the displacement of the moving basis) on the radial nonadiabatic transitions discussed above and will therefore be removed. Consequently, from expression (20) one can observe that the radial nonadiabatic coupling vanishes for $R \to \infty$ because $\partial G_0(E_{indx,\Omega})/\partial R = -\partial E_{indx,\Omega}/\partial R \cdot G_0^2(E_{indx,\Omega}) \to 0$ and $\partial C_{s\nu}^{\Omega}/\partial R \to 0$ when the molecular sp states approach the fixed sp states of the separated nuclei. In Appendix A we give expressions for the calculation of the actual radial nonadiabatic coupling matrix elements including the first four terms of (20) only.

After diagonalizing the actual radial nonadiabatic coupling we obtain the unitary transformation matrix S_{ij}^{Ω} between the adiabatic and diabatic representations, where i, j refer to the values of $indx$. The diabatic sp wave functions and energy levels are obtained as follows

$$|i \ \Omega>_{diab}= \sum_j s_{ij}^{\Omega} \ |j \ \Omega>_{adiab}, \tag{21}$$

$$E_{i\Omega}^{diab} = \sum_j |s_{ij}^{\Omega}|^2 E_{j\Omega}^{adiab}. \tag{22}$$

8

For a given Ω the adiabatic sp levels $E_{i\Omega}^{adiab}$ as a function of R (correlation diagram [22]) show avoided crossings because of the noncrossing rule by von Neumann and Wigner [21], while the diabatic levels $E_{i\Omega}^{diab}$ reveal real crossings. The diabatic states (21)-(22) can cross each other because they are not solutions of an eigenvalue problem.

There are approximating methods [22] for calculating diabatic states, namely the maximum symmetry method and the maximum overlap method. These techniques were applied in Ref. [23] to obtain diabatic states with a TCSM based on harmonic oscillators. In Refs. [17,24] we made use of the maximum symmetry method to calculate diabatic potential energy surfaces of near symmetric reactions. Other methods have been developed in quantum chemistry for the calculation of such a diabatic basis, e.g., see Ref. [25].

3 Numerical results

As an example of the realistic TCSM discussed above we present calculations for neutrons and protons in the reaction ^{16}O + ^{40}Ca $\rightarrow$ ^{56}Ni. The potential parameters for the separated nuclei and the compound nucleus as well as the maximal number of nodes n_{max} and partial waves l_{max} included in the harmonic oscillator basis for converged values of the sp energies are given in Table 1. These parameters approximately reproduce the experimental sp levels around the Fermi energy, which was shown in Refs. [6,26].

3.1 Neutrons

Fig. 1 shows the function $y(R)$ derived from the condition of volume conservation for different values of the α parameter which determines both the partition of the compound nucleus potential depth into two parts belonging to each fragment and their charges. The numerically calculated function $y(R)$ is used in expression (6) to interpolate the two-center potential parameters. It is observed that (i) $y(R)$ decreases from 1 around the contact configuration ($R \approx 7.3$ fm) up to 0 for the spherical compound nucleus ($R = 0$ fm), and (ii) $y(R)$ very strongly depends on the α parameter at small radii R, while this is not the case around the contact point. The strong effect of the α parameter on the neutron sp spectra at small distances R can be seen in Fig. 2.

In Fig. 2 we show normalized neutron sp levels with $\Omega = 1/2$ as a function of the quadrupole deformation parameter β of the ^{56}Ni compound nucleus for two values of the α parameter, namely $\alpha = 0.4$ (right panel) and $\alpha = 0.8$ (middle panel). Moreover, these level diagrams are compared to the levels of

Table 1

Potential parameters for the separated nuclei and the compound nucleus: The potential depth is given in MeV, the radii and diffusenesses in fm, while the strength λ of the spin-orbit potential is adimensional. The radii $R_{0(so)} = r_{0(so)}A^{1/3}$ being A the mass number of the nucleus. See text for further details.

Nucleus	V_0	r_0	a_0	λ	r_{so}	a_{so}	R_c	n_{max}	l_{max}
Neutrons									
^{16}O[a]	74.90	0.97	0.60	19.50	1.10	0.55		4	3
^{40}Ca[a]	51.40	1.28	0.76	24	1.37	0.55		4	3
^{56}Ni[b]	46.20	1.31	0.62	18.73	1.31	0.62		4	3
Protons									
^{16}O[a]	79.10	0.95	0.59	19.15	1.10	0.55	2.77	4	3
^{40}Ca[a]	70.80	1.05	0.67	19.22	1.05	0.55	3.83	4	3
^{56}Ni[b]	53.70	1.24	0.63	13.97	1.31	0.63	4.74	4	3

[a]From Ref. [6], [b]From Ref. [26]

the Nilsson model [27] (left panel). The normalization is given by the first Nilsson-level and the β value is obtained from the quadrupole moment of the nuclear shape. From this figure it is concluded that a realistic value of α is about 0.8 because, as expected, the behaviour of the two-center sp levels is similar to that in the Nilsson model. In the following we will use $\alpha = 0.8$.

Fig. 3 shows the central part of the neutron two-center potential along the z-axis for fixed values of the distance R between the fragments. The nuclear shape associated with each potential is also included in this figure. Near the contact configuration ($R = 7$ fm) the interfragment potential barrier practically disappears and, therefore, most of the nucleons may move in the whole volume of the system. From distances $R \lesssim 4$ fm the two-center potential essentially adopts a one-center character. It is worth mentioning that the two-center potential barrier is naturally formed in the present model by the superposition of the tail of the two WS potentials.

Fig. 4 shows the adiabatic (left panel) and diabatic (right panel) neutron levels with $\Omega = 1/2$ as a function of the internuclear distance R. For small and large radii we can observe the shell structure of the compound nucleus and the separated fragments, respectively. For distances 3 fm $\lesssim R \lesssim 7$ fm sp levels are strongly polarized and the shell structure of the separated fragments is practically dissolved. Here sp excitations and transfer processes essentially occur around the avoided crossing of the molecular adiabatic sp levels due to the effect of the radial nonadiabatic couplings on the sp motion. Most of the
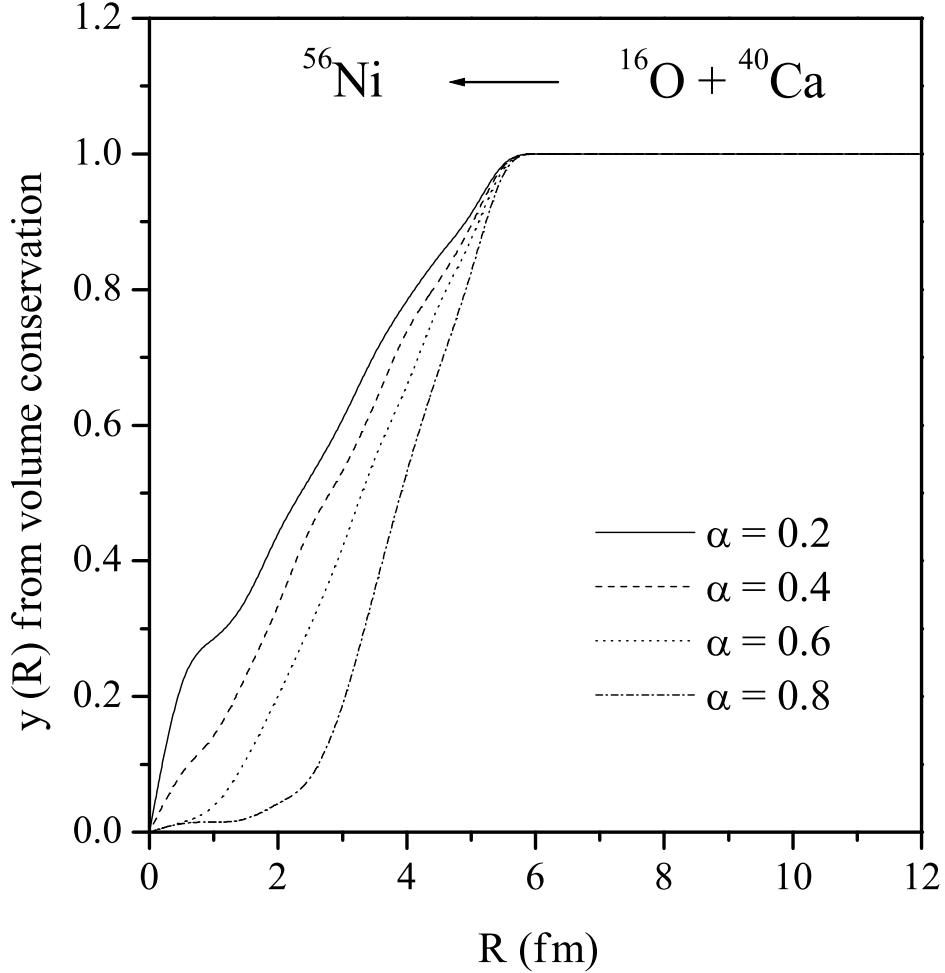
Fig. 1. The function $y(R)$ derived from the condition of volume conservation for different values of the α parameter. This is used to interpolate the neutron and proton two-center potential parameters as a function of the radius R between the nuclei. See text for further details.

avoided crossings in the adiabatic level diagram turn into real crossings in the diabatic level diagram. This happens where the radial nonadiabatic coupling between the adiabatic sp levels shows huge peaks which can be seen in Fig. 5.

Fig. 5 shows the absolute value of the radial nonadiabatic couplings between some neighbouring adiabatic levels of Fig. 4 (left panel) as a function of the internuclear radius: levels 3-4 (solid curve), levels 5-6 (dotted curve) and levels 8-9 (dashed curve). For large distances the couplings vanish as expected. The more bound the levels are, the smaller is the radius R in which the coupling vanishes, e.g., comparing levels 3-4 (solid curve) and levels 8-9 (dashed curve).
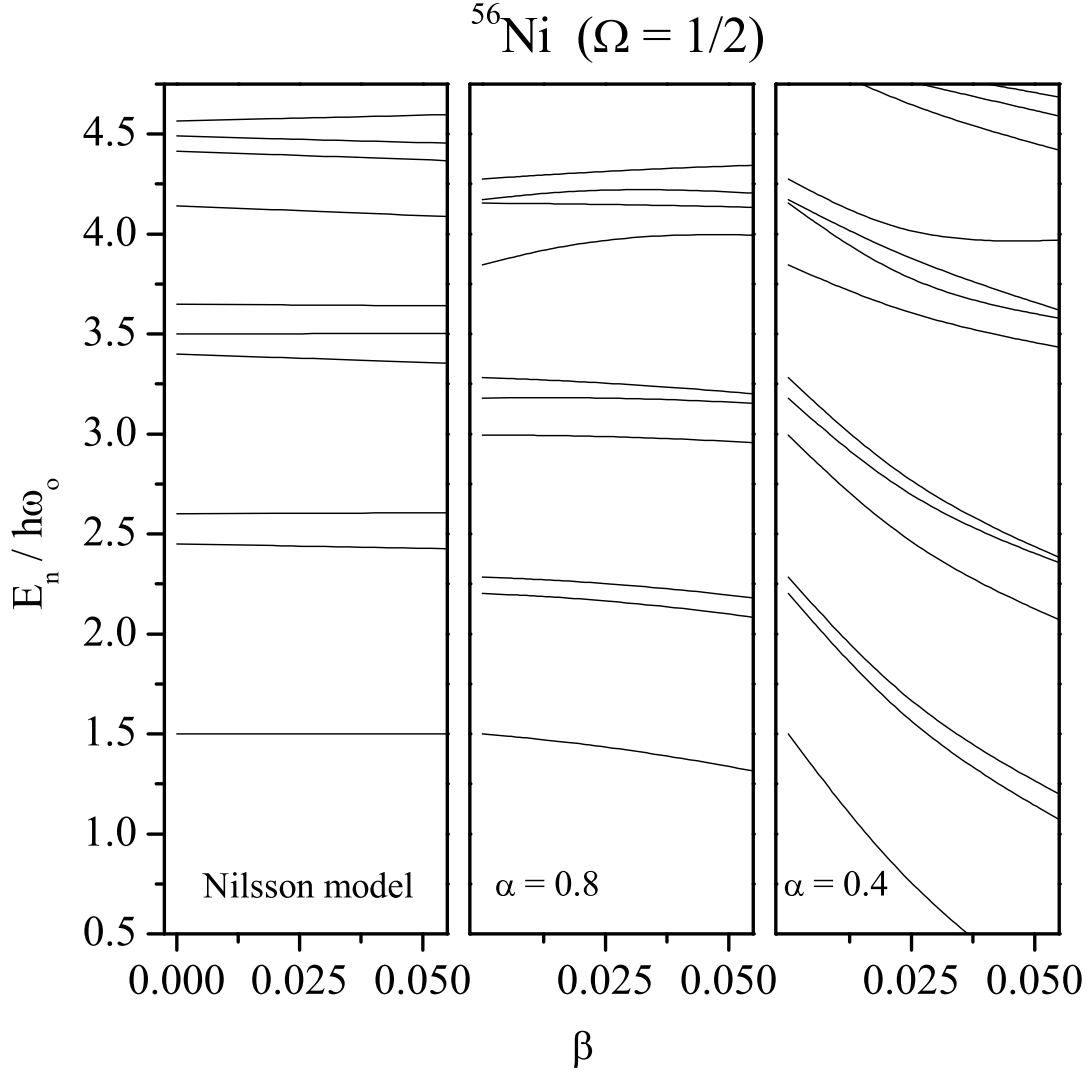
11

Fig. 2. Normalized neutron levels with $\Omega = 1/2$ as a function of the quadrupole deformation β of the compound nucleus ^{56}Ni for different values of the α parameter: $\alpha = 0.4$ (right panel) and $\alpha = 0.8$ (middle panel). The left panel shows the levels of the Nilsson model. See text for further details.

The huge peaks localize the position of an avoided crossing where a nucleon transition (Landau-Zener effect) may occur with a large probability. These peaks are the key to calculating the diabatic states which are obtained by minimizing those strong couplings only. The threshold value for the strength of the couplings was $\gamma_{thr} = 1.4$. It is important to stress that strong transitions between molecular sp levels as that between the levels 8-9 (dashed curve) at $R \approx 8$ fm can also occur for distances larger than that in the contact configuration. In these situations Landau-Zener nucleon transitions may be reflected in the excitation function of direct reaction processes [3].
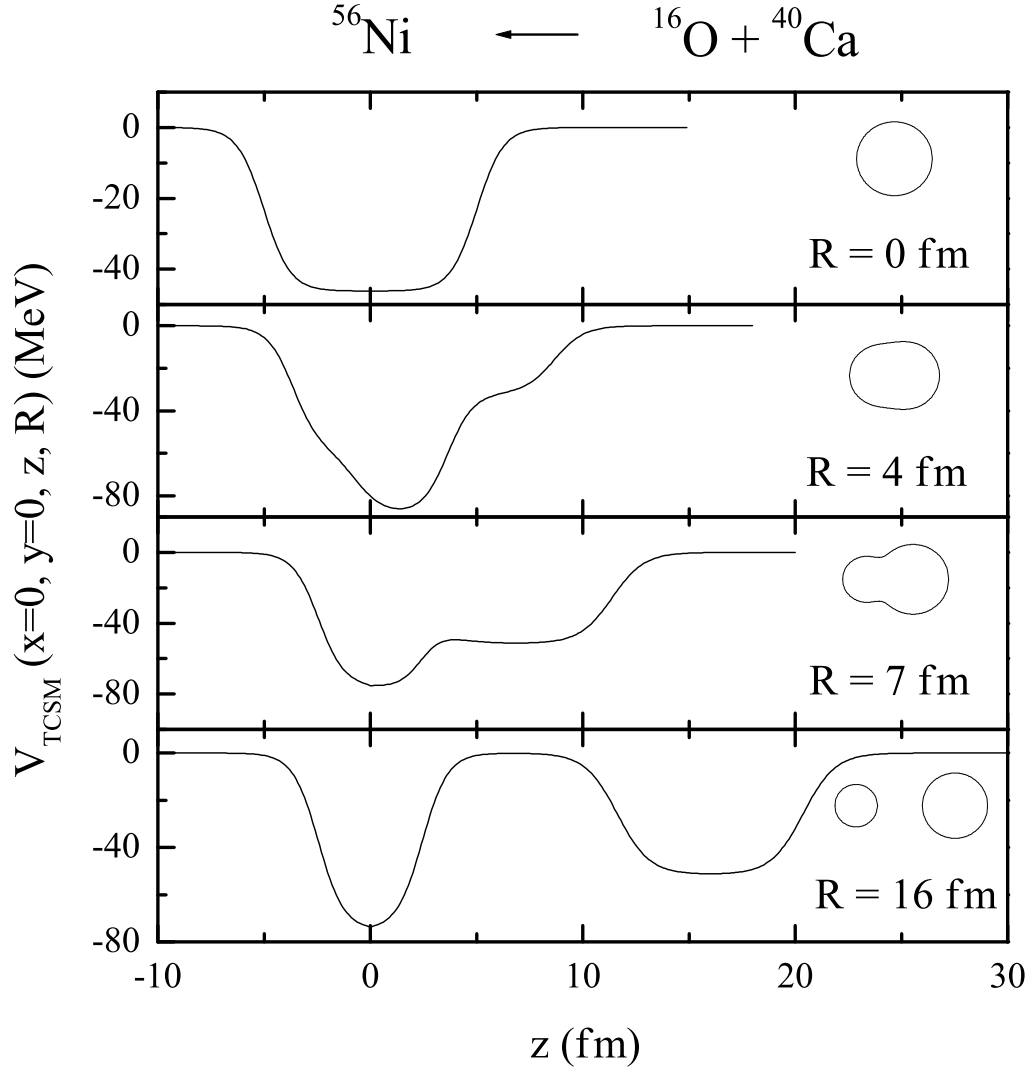
Fig. 3. The central part of the neutron two-center potential along the z-axis for fixed radii R between the nuclei. The nuclear shape associated with each potential is also included. See text for further details.

In Fig. 6, the adiabatic neutron levels correlation diagram including all bound states with different Ω values is presented, i.e., $\Omega = 1/2$ (solid curves), $\Omega = 3/2$ (dashed curves), $\Omega = 5/2$ (dotted curves) and $\Omega = 7/2$ (dashed-dotted-dotted curve). The states with the same Ω value are coupled by the radial coupling discussed above, while those states with Ω values differing by one unit in Ω (e.g., $\Omega = 1/2$ and $\Omega = 3/2$) are coupled in the laboratory reference frame by the so-called rotational (or Coriolis) coupling which is maximal at the real crossing of these states [3].

Both the adiabatic and the diabatic sp states with different Ω values, as mentioned above, are coupled in the laboratory system by the rotational coupling.

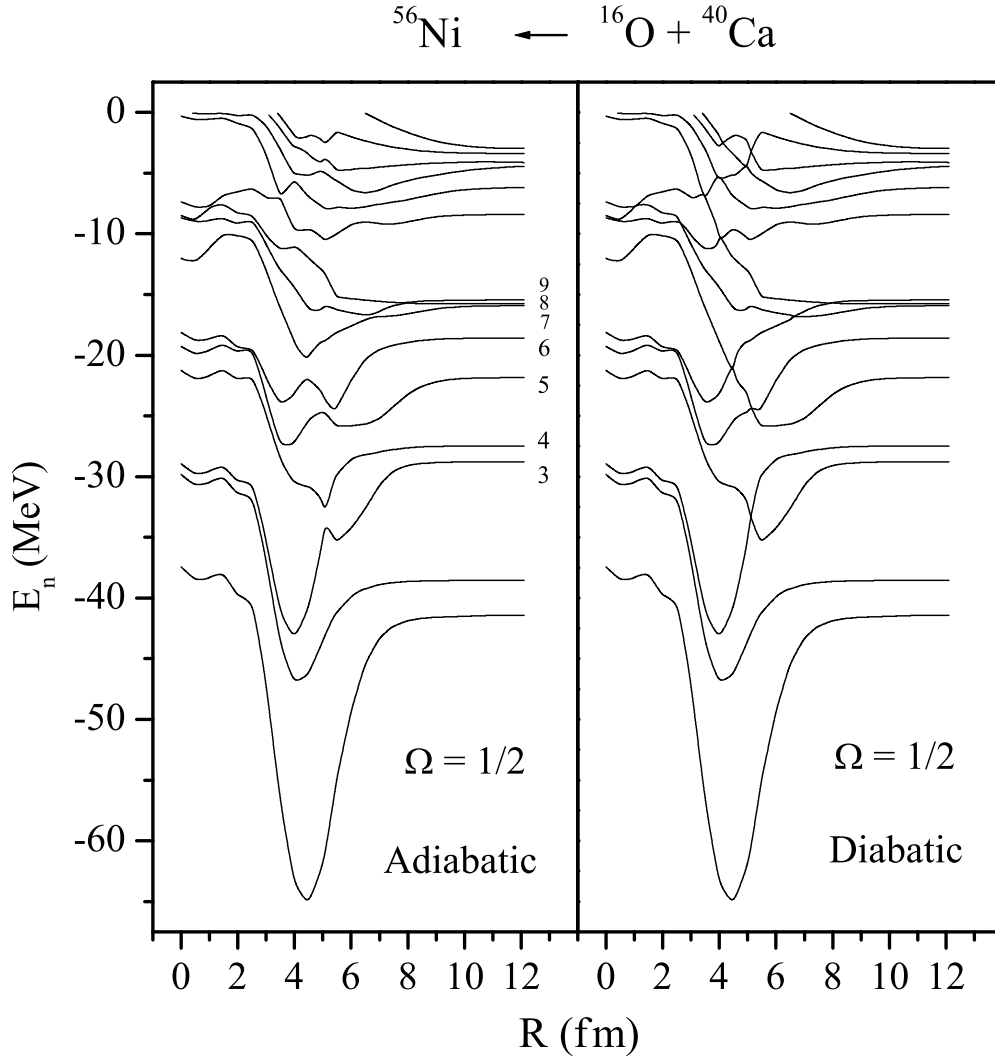^{56}Ni $\longleftarrow$ ^{16}O + ^{40}Ca

Fig. 4. Adiabatic (left panel) and diabatic (right panel) neutron levels with $\Omega = 1/2$ as a function of the radius R between the nuclei. Some adiabatic levels are labeled by 3-9. See text for further details.

The rotational coupling ($\sim \mathbf{j} \cdot \mathbf{I}$, where $\mathbf{j}$ is the nucleon total angular momentum and $\mathbf{I}$ is the total angular momentum of the system) appears in a non central collision due to the rotation of the molecular internuclear axis with respect to a space-fixed axis. Please note that the sp wave-functions ((18) and (21)) depend on the Wigner rotation matrices. One can expect that the rotational coupling (which increases with decreasing internuclear radii R, i.e., $\sim 1/R^2$) is important in light ion collisions owing to the small moment of inertia of the system, but it is not the case in a heavy ion reaction. In fusion of light systems (where the fusion process is already determined by the penetration of the external Coulomb barrier, i.e., small overlap between the nuclei) the relevant radial region for the rotational coupling is governed by the usually
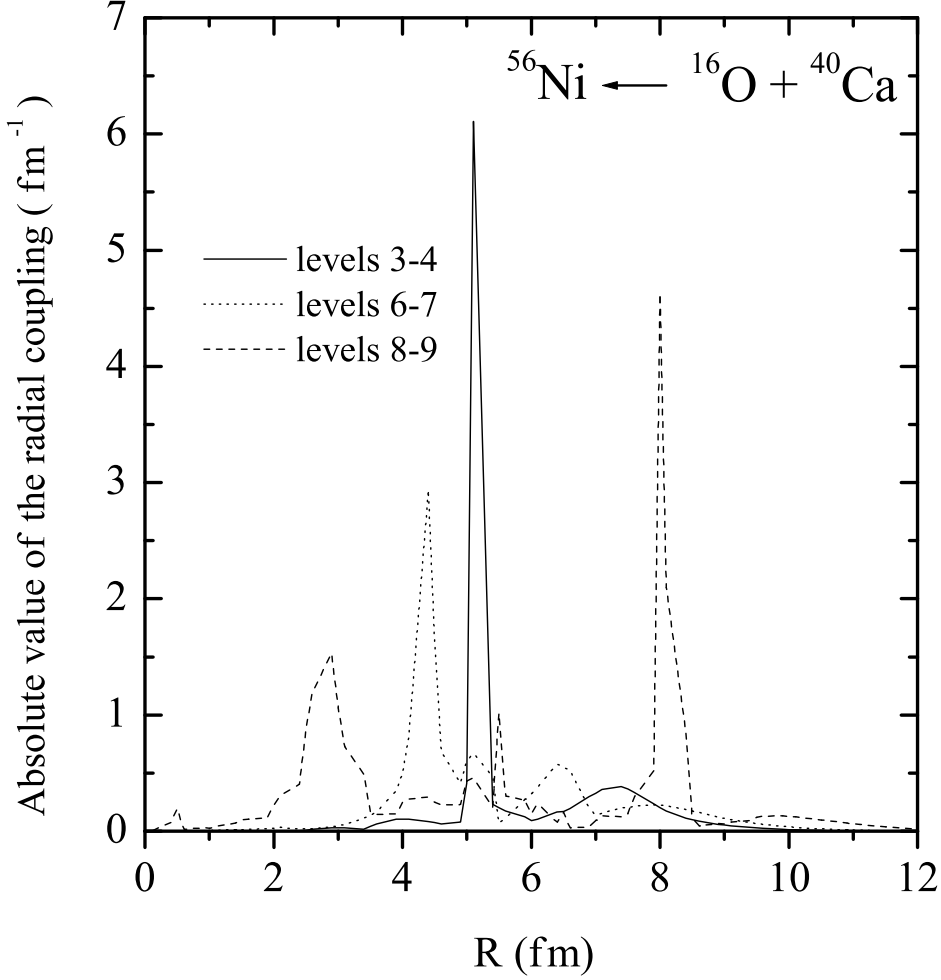
14

Fig. 5. Absolute value of the radial nonadiabatic coupling between some neighbouring adiabatic levels of Fig. 4 (left panel) as a function of the radius R between the nuclei. See text for further details.

strongly absorptive nucleus-nucleus potential. Terlecki et al. [28] have found in the reaction ^{13}C+^{13}C that the effect of the rotational coupling on the inelastic excitation cross sections is much smaller than the effect of the radial coupling. We would like to add that Imanishi and von Oertzen have introduced in Ref. [29] the so-called Rotating Molecular Orbitals (RMO) in the standard coupled reaction channels formalism in order to avoid numerical problems with the rotational coupling at small internuclear radii R. To our knowledge, there has been no systematic study of the effect of rotational couplings on fusion and scattering cross sections. Further work on this issue is required.
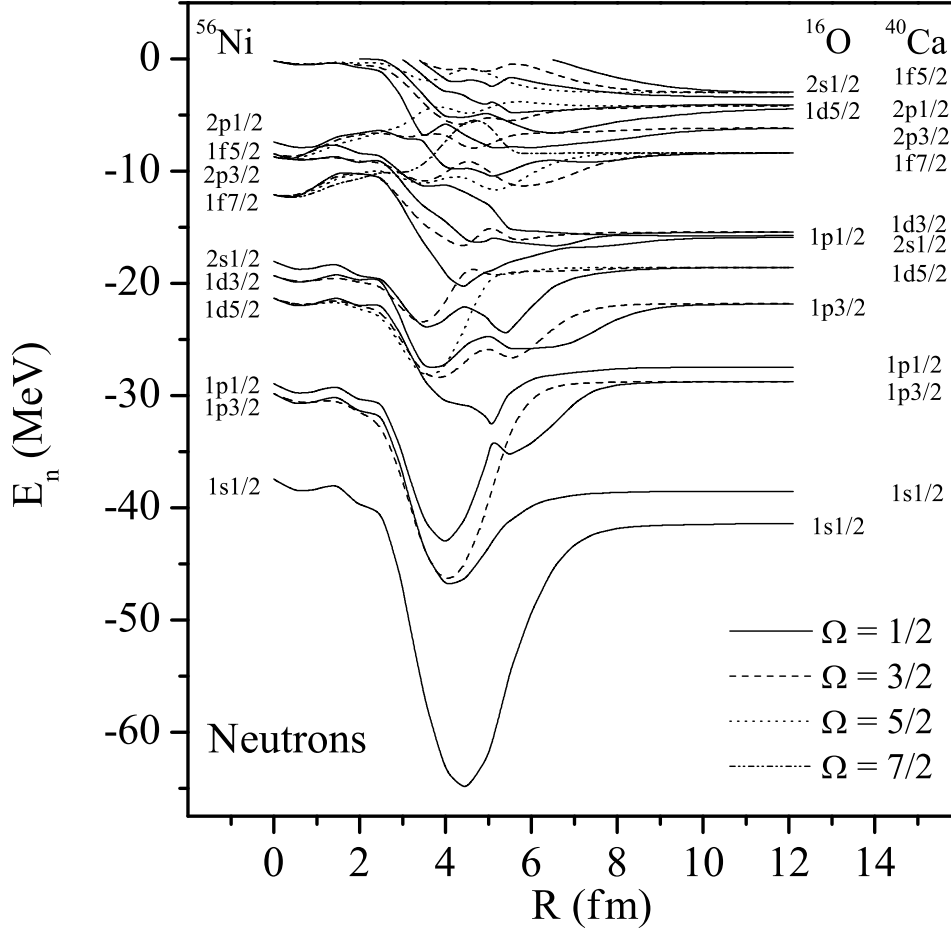
Fig. 6.

Fig. 7. The adiabatic neutron levels correlation diagram including all bound states with different Ω values. See text for further details.

3.2   Protons

Since we have assumed that the nuclear shape is the same for neutrons and protons, the same function $y(R)$ of Fig. 1 ($\alpha = 0.8$, dashed-dotted curve) is applied in interpolating the proton two-center potential parameters. In Fig. 7 like in Fig. 3, the central part of the proton two-center potential along the z-axis is shown for different fixed internuclear distances R. Apart from (i) the positive tails of the two-center potential for large z values due to the Coulomb interaction and (ii) a higher barrier between the fragments at $R = 7$ fm, the change of the two-center potential with R is similar to that in Fig. 3 for

16

^{56}Ni ⟵ $^{16}\text{O} + {}^{40}\text{Ca}$

R = 0 fm

R = 4 fm

R = 7 fm

R = 16 fm

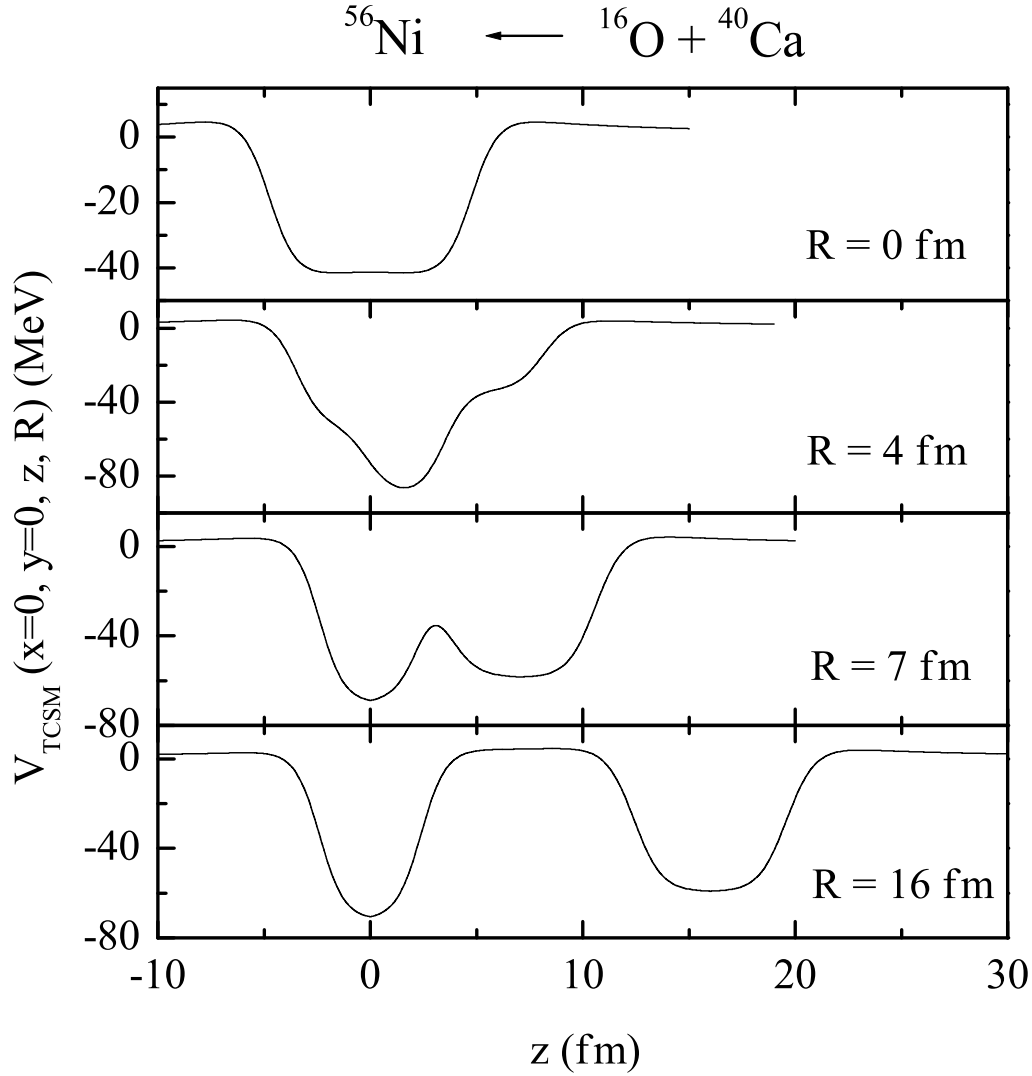V_{TCSM} (x=0, y=0, z, R) (MeV)

z (fm)

Fig. 8. The same as Fig. 3, but for protons. See text for further details.

neutrons. Fig. 8 shows the adiabatic (left panel) and diabatic (right panel) correlation diagram of the proton levels with $\Omega = 1/2$. The same features as those observed for neutrons in Fig. 4 can be seen here. In order to isolate the strong peaks of the proton radial nonadiabatic coupling, a threshold value $\gamma_{thr} = 1.7$ for the strength of the couplings was needed in this case to calculate the diabatic levels. Fig. 9 is like Fig. 6, but for protons. The level diagram shows similar features as those in Fig. 6, only the levels are shifted up due to the Coulomb interaction.
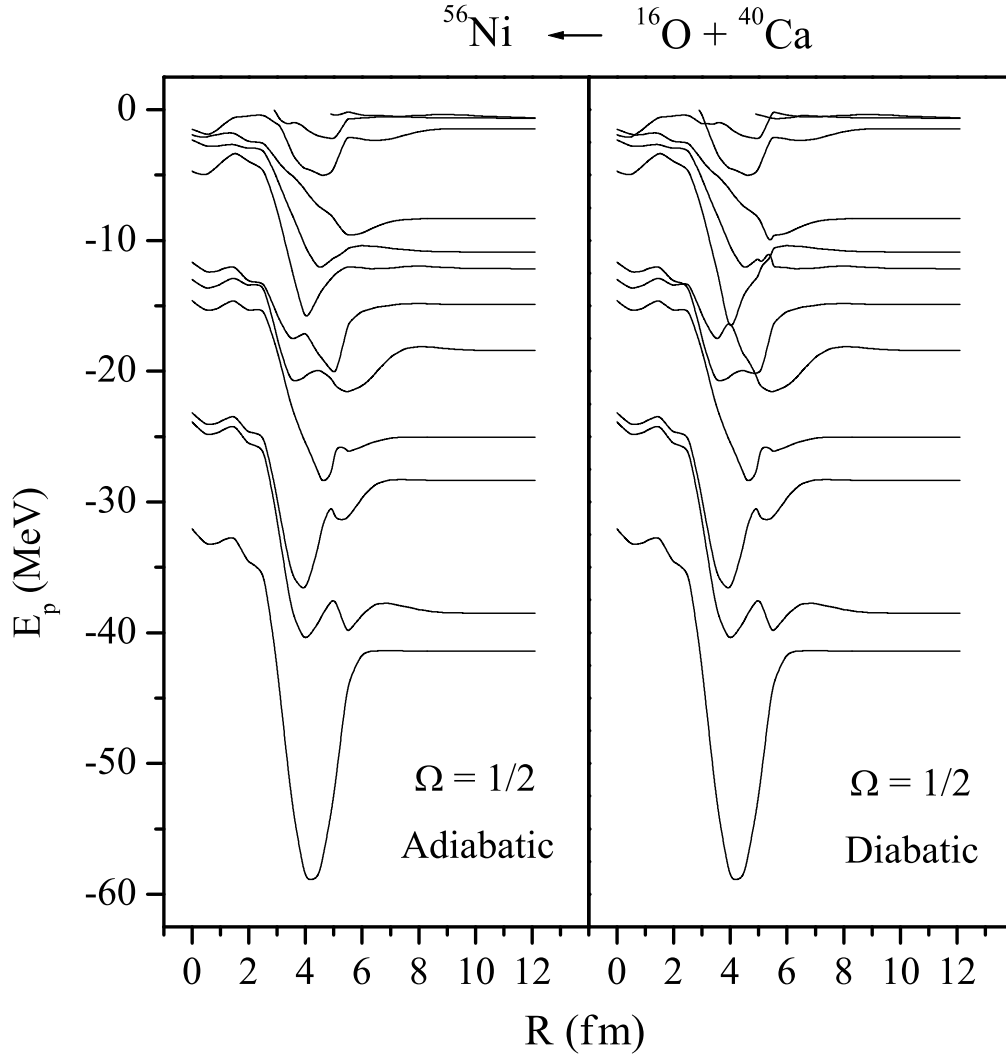
$$^{56}\text{Ni} \quad \longleftarrow \quad ^{16}\text{O} + {}^{40}\text{Ca}$$

Fig. 9. The same as Fig. 4, but for protons. See text for further details.

4 Concluding remarks

A realistic TCSM for fusion has been proposed, which is based on two spherical WS potentials and the PSE method. This model describes the sp motion in a fusing system. The adiabatic and diabatic molecular sp states for neutrons and protons in the reaction $^{16}\text{O} + {}^{40}\text{Ca} \rightarrow {}^{56}\text{Ni}$ have been calculated. A technique to compute the stationary diabatic states has been introduced, which is based on the minimization of the strong radial nonadiabatic coupling between the adiabatic states. The only difference between the stationary diabatic sp basis and the adiabatic one is that the diabatic basis minimizes the strong radial nonadiabatic coupling localized at some of the avoided crossings between the adiabatic levels. Whether it is more convenient to use either the
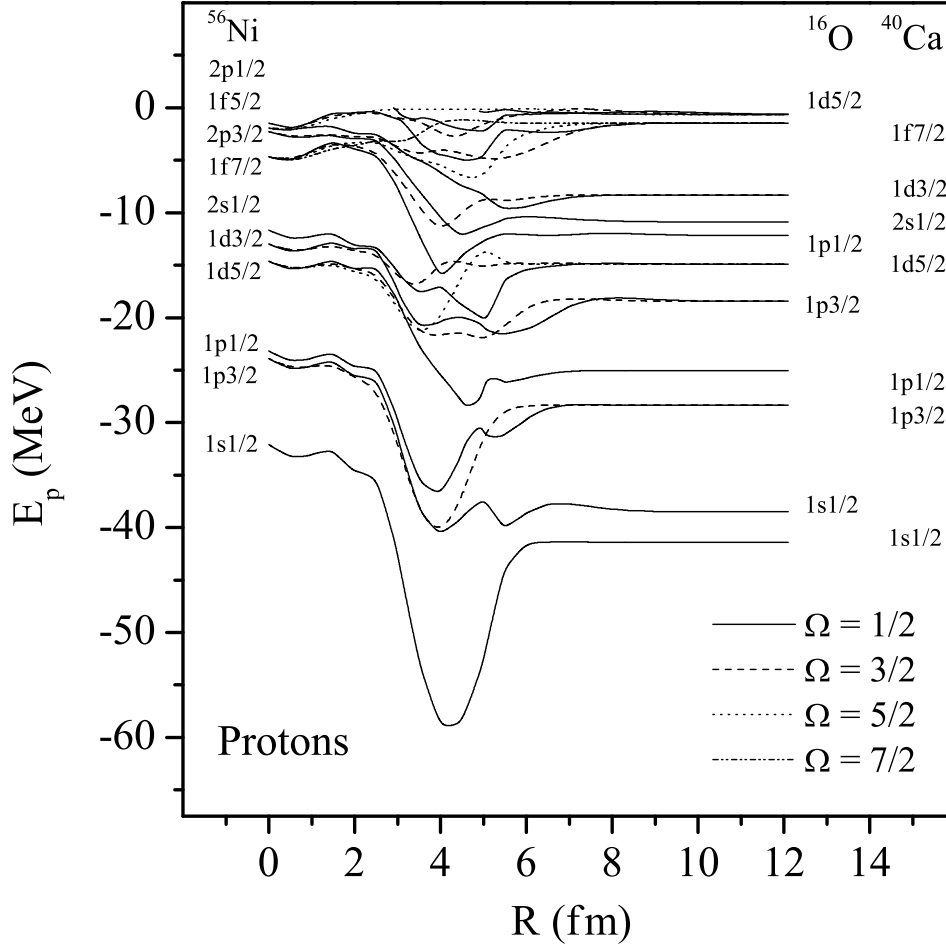
Fig. 10. The same as Fig. 6, but for protons. See text for further details.

adiabatic or the diabatic basis essentially depends on the bombarding energy [16]. It is important to add that the *dynamical* radial nonadiabatic coupling is proportional to the ion-ion radial velocity $\dot{R}$ which modulates the stationary (or static) couplings calculated in the present work.

At very low incident energies (e.g., energies below the Coulomb barrier) one can expect that the real sp motion is well described by the adiabatic representation. The dynamics of the sp motion becomes even simpler when the dynamical nonadiabatic couplings may be neglected and so the nucleons remain at the lowest energy levels. When the incident energy increases, the dynamical couplings are more and more strengthened. In this case, nucleon transitions between the adiabatic molecular sp levels occur. The adiabatic basis along with all nonadiabatic couplings should then be used for understanding the real sp

19

motion. If the incident energy reaches a certain value (e.g., 1 MeV/u above the Coulomb barrier for heavy symmetric systems [16]) at which the dynamical nonadiabatic coupling is very strong (probability of the nucleon transition is close to one), then the diabatic sp basis approximates the real sp motion. At this energy regime, the use of the diabatic basis is certainly very useful to simplify the dynamical calculation. It is worth mentioning that the diabatic sp motion is expected to be realistic in the entrance phase of heavy-ion reactions [16]. The adiabatic and diabatic representations can be used as sp bases in a coupled channels calculation within a molecular quantum-mechanical formulation of heavy ion collisions [3,29]. Works regarding the application of the present TCSM in understanding the formation mechanism of superheavy elements are in progress.

A Actual radial nonadiabatic coupling matrix elements

The matrix elements $< indx\ \Omega|\partial/\partial R|indx'\ \Omega >$ can be calculated as follows including only the first four terms of (20) (for clarity Ω will be removed, and new α and β indexes will refer to $indx$ and $indx'$, respectively)

$$< \alpha|\frac{\partial}{\partial R}|\beta >= term1 + term2 + \cdots + term8, \tag{A.1}$$

where

$$term1 = \sum_{\nu'=1}^{N_1} \sum_{\nu=1}^{N_1} C_{1\nu'}^* < 1\nu'|\ G_0(E_\alpha)G_0(E_\beta)\ |1\nu > \frac{\partial C_{1\nu}}{\partial R}, \tag{A.2}$$

$$term2 = \sum_{\nu'=1}^{N_2} \sum_{\nu=1}^{N_2} C_{2\nu'}^* < 2\nu'|\ G_0(E_\alpha)G_0(E_\beta)\ |2\nu > \frac{\partial C_{2\nu}}{\partial R}, \tag{A.3}$$

$$term3 = \sum_{\nu'=1}^{N_1} \sum_{\nu=1}^{N_1} C_{1\nu'}^* < 1\nu'|\ G_0(E_\alpha)\frac{\partial G_0(E_\beta)}{\partial R}\ |1\nu > C_{1\nu}, \tag{A.4}$$

$$term4 = \sum_{\nu'=1}^{N_2} \sum_{\nu=1}^{N_2} C_{2\nu'}^* < 2\nu'|\ G_0(E_\alpha)\frac{\partial G_0(E_\beta)}{\partial R}\ |2\nu > C_{2\nu}, \tag{A.5}$$

$$term5 = \sum_{\nu'=1}^{N_1} \sum_{\nu=1}^{N_2} C_{1\nu'}^* < 1\nu'|\ G_0(E_\alpha)G_0(E_\beta)e^{i\mathbf{R}\hat{k}}\ |2\nu > \frac{\partial C_{2\nu}}{\partial R}, \tag{A.6}$$

$$term6 = \sum_{\nu'=1}^{N_2} \sum_{\nu=1}^{N_1} C_{2\nu'}^* < 2\nu'| \, G_0(E_\alpha) G_0(E_\beta) e^{-i\mathbf{R}\hat{k}} \, |1\nu > \frac{\partial C_{1\nu}}{\partial R}, \qquad (A.7)$$

$$term7 = \sum_{\nu'=1}^{N_1} \sum_{\nu=1}^{N_2} C_{1\nu'}^* < 1\nu'| \, G_0(E_\alpha) \frac{\partial G_0(E_\beta)}{\partial R} e^{i\mathbf{R}\hat{k}} \, |2\nu > C_{2\nu}, \qquad (A.8)$$

$$term8 = \sum_{\nu'=1}^{N_2} \sum_{\nu=1}^{N_1} C_{2\nu'}^* < 2\nu'| \, G_0(E_\alpha) \frac{\partial G_0(E_\beta)}{\partial R} e^{-i\mathbf{R}\hat{k}} \, |1\nu > C_{1\nu}. \qquad (A.9)$$

The matrix elements contained in $term1$ and $term2$ (i.e., $< s\nu'| \, G_0(E_\alpha) G_0(E_\beta) \, |s\nu >$ with $s = 1, 2$) are obtained using both the relation

$$G_0(E_\alpha) G_0(E_\beta) = \frac{1}{(E_\alpha - E_\beta)} [G_0(E_\alpha) - G_0(E_\beta)], \ E_\alpha \neq E_\beta \qquad (A.10)$$

and the matrix elements given by expression (12).

The matrix elements of $term3$ and $term4$ are calculated applying the relation

$$< s\nu'| \, G_0(E_\alpha) \frac{\partial G_0(E_\beta)}{\partial R} \, |s\nu > = \frac{\partial E_\beta}{\partial R} \frac{\partial}{\partial E_\beta} < s\nu'| \, G_0(E_\alpha) G_0(E_\beta) \, |s\nu > . \qquad (A.11)$$

The rest of the matrix elements involved in $term5, \cdots, term8$ are obtained making use of (i) the relation (A.10), (ii) the matrix elements calculated with expression (13), and (iii) the derivative rule used in the relation (A.11).

References

[1] P. Holzer, U. Mosel and W. Greiner, Nucl. Phys. A **138**(1969) 241.

[2] J.A. Maruhn and W. Greiner, Z. Phys. **251**(1972) 431.

[3] W. Greiner, J.Y. Park and W. Scheid, in *Nuclear Molecules* (World Scientific, Singapore, 1994).

[4] M. Mirea, Phys. Rev. C **54**(1996) 302.

[5] R.A. Gherghescu, Phys. Rev. C **67**(2003) 014309.

[6] K. Pruess and P. Lichtner, Nucl. Phys. A **291**(1977) 475.

[7] G. Nuhn, W. Scheid and J.Y. Park, Phys. Rev. C **35**(1987) 2146.

[8] J. Revai, JINR, E4-9429, Dubna (1975).

[9] B. Gyarmati, A.T. Kruppa and J. Revai, Nucl. Phys. A **326**(1979) 119.

[10] F.A. Gareev, M.Ch. Gizzatkulov and J. Revai, Nucl. Phys. A **326**(1977) 512.

[11] B. Milek and R. Reif, Phys. Lett. B **157**(1985) 134; Nucl. Phys. A **458**(1986) 354.

[12] F.A. Gareev, S.N. Ershov, J. Revai, J. Bang and B.S. Nilsson, Phys. Scripta **19**(1979) 509.

[13] B. Gyarmati and A.T. Kruppa, Nucl. Phys. A **378**(1982) 407; B. Gyarmati, A.T. Kruppa, Z. Papp and G. Wolf, Nucl. Phys. A **417**(1984) 393.

[14] A.C. Fonseca, J. Revai and A. Matveenko, Nucl. Phys. A **326**(1979) 182; J. Revai and A. Matveenko, Nucl. Phys. A **339**(1980) 448.

[15] J.B. Delos and W.R. Thorson, J. Chem. Phys. **70**(1979) 1774; Rev. Mod. Phys. **53**(1981) 287.

[16] W. Cassing and W. Nörenberg, Nucl. Phys. A **433**(1985) 467.

[17] A. Diaz-Torres, Phys. Rev. C **69**(2004) 021603(R).

[18] A. Diaz-Torres, Phys. Lett. B **594**(2004) 69.

[19] P. Ring and P. Schuck, in *The Nuclear Many-Body Problem* (Springer-Verlag, New York Inc., 1980) p. 41.

[20] D.A. Varshalovich, A.N. Moskalev and V.K. Khersonskii, in *Quantum Theory of Angular Momentum* (World Scientific, Singapore, 1989).

[21] J. von Neumann and E. Wigner, Z. Physik **30**(1929) 467.

[22] E.E. Nikitin and S.Ya. Kmanskii, in *Theory of Slow Atomic Collisions* (Springer-Verlag, Berlin, 1984) p.74.

[23] A. Lukasiak, W. Cassing and W. Nörenberg, Nucl. Phys. A **426**(1984) 181.

[24] A. Diaz-Torres, N.V. Antonenko and W. Scheid, Nucl. Phys. A **652**(1999) 61.

[25] A. Troisi and G. Orlandi, J. Chem. Phys. **118**(2003) 5356, and references therein.

[26] V.G. Soloviev, in *Theory of Atomic Nuclei (Nuclear Models)* (Energoizdat, Moscow, 1981) p.67.

[27] J.M. Irvine, in *Nuclear Structure Theory* (Pergamon Press, Oxford, 1972) p.313.

[28] G. Terlecki, W. Scheid, H.J. Fink and W. Greiner, Phys. Rev. C **18**(1978) 265.

[29] B. Imanishi and W. von Oertzen, Phys. Rep. **155**(1987) 29.